Nanoscale

Cite this: DOI: 10.1039/c1nr11260k

www.rsc.org/nanoscale

PAPER

Comparative analysis of nanomechanics of protein filaments under lateral loading

Max Solar[ab] and Markus J. Buehler*[a]

Received 7th September 2011, Accepted 31st October 2011
DOI: 10.1039/c1nr11260k

Using a combination of explicit solvent atomistic simulation and continuum theory, here we study the lateral deformation mechanics of three distinct protein structures: an amyloid fibril, a beta helix, and an alpha helix. We find that the two β-sheet rich structures – amyloid fibril and beta helix, with persistence lengths on the order of μm – are well described by continuum mechanical theory, but differ in the degree to which shear deformation affects the overall bending behavior. The alpha helical protein structure, however, with a persistence length on the order of one nanometer, does not conform to the continuum theory and its deformation is dominated by entropic elasticity due to significant fluctuations. This study provides fundamental insight into the nanomechanics of widely found protein motifs and insight into molecular-scale deformation mechanisms, as well as quantitative estimates of Young's modulus and shear modulus in agreement with experimental results.

1. Introduction

The secondary structure of proteins is a distinguishing feature of different protein materials, and can be experimentally measured using techniques such as X-ray crystallography and nuclear magnetic resonance spectroscopy.[1–3] Not so clear, however, is the relationship between the secondary structure type, the size of the structure and the resulting mechanical properties under different loading conditions. Here we explore the nanomechanics of filamentous protein structures under lateral loading similar to bending to identify key mechanical parameters such as the Young's modulus, the shear modulus, and the bending rigidity. We consider three protein structures each with unique defining geometric characteristics: the Aβ(1–40) amyloid fibril, a β-helical nanotube, and an alpha helix.

The Aβ(1–40) amyloid fibril is one of a large class of amyloid structures that are widely known to be associated with neurodegenerative diseases including Alzheimer's disease, Parkinson's disease and type II diabetes.[4,5] This and other amyloid structures have also been considered excellent candidate materials for functional roles due to their good mechanical properties and self-assembling nature.[5–7] Recent computational work has examined the behavior of the Aβ(1–40) fibril under tensile and compressive loading,[8–15] however lateral loading and bending behavior have not been extensively studied. Further, β-helices, also known as β-solenoids, are commonly compared to amyloid structures, and have also been proposed for use in functional roles.[16] Both the amyloid fibril and the β-helix are characterized by their high β-sheet content, but they feature a key difference; in the amyloid fibril, individual layers are held together only by hydrogen bonds, but in the β-helix, a continuous covalently bonded backbone exists in addition to the hydrogen bonded β-sheets. Again, the β-helix structure has been studied under compressive and tensile loading,[17] but not under lateral loading. Finally, the alpha helix structure considered represents a filamentous protein structure on a smaller size scale than the aforementioned β-sheet rich structures. Previous work has examined the mechanical behavior of alpha helices,[18] however the large difference in size between the β-sheet rich structures and the alpha helix provides an opportunity to directly compare the effect of secondary structure dimension on the mechanical properties.

Here we use full atomistic, explicit solvent molecular dynamics methods to apply lateral force loading to each of the three previously described protein structures. We perform a detailed study of their deformation behavior, including analyzing the different contributions to bending deformation, as well as comparing the results to predictions from continuum mechanical theory. Based on our simulation results we propose that for structures with lengths well below their persistence length, continuum mechanical theory will well describe the deformation behavior. In contrast, for structures with lengths greater than their persistence length, continuum theory will fail to accurately predict deformation behavior, and a statistical description of the behavior will be required.

[a]*Laboratory for Atomistic and Molecular Mechanics (LAMM), Department of Civil and Environmental Engineering, Massachusetts Institute of Technology, 77 Massachusetts Ave., Cambridge, MA, USA. E-mail: mbuehler@MIT.EDU*
[b]*Department of Materials Science and Engineering, Massachusetts Institute of Technology, 77 Massachusetts Ave., Cambridge, MA, USA*

2. Materials and methods

2.1 Molecular dynamics models

Two widely found β-sheet rich protein structures are considered in this study: amyloid protein fibrils comprising individual layers stacked upon each other and held together by hydrogen bonds between β-sheets, as well as β-helices which have a continuous covalently bonded backbone and β-sheets parallel to the helix axis. Two-fold symmetric Aβ (1–40) amyloid fibrils are built according to [19] with lengths ranging from 1.92 to 9.58 nm. Fig. 1(a) shows a 3.83 nm Aβ fibril. Parallel left-handed β-helix structures are built with coordinates obtained from the Protein Data Bank (identification code 1FWY).[20,21] Residues 276–311 are copied and translated up the helix axis to form a continuous backbone as shown in Fig. 1(b). Structures ranging from 6 to 20 turns are investigated, corresponding to lengths of 3.73 to 10.72 nm. Additionally, an alpha helix structure is considered as a comparison to the two β-sheet rich structures. Initial coordinates are taken from the Protein Data bank (identification code 1GK6),[20,22] and a segment comprising ten residues (2.3 nm) is taken for this study. The choice of ten residues is motivated by recent work which suggests that alpha helices of this length are most stable to self-unfolding or formation of tertiary structures.[23]

For all structures, the protein structure and coordinate files are created using tools in VMD[24] and NAMD[25] with CHARMM topology and force-field parameter files.[26] All simulations are performed with periodic boundary conditions in explicit water boxes with system sizes ranging from approximately 6,000 to 100,000 atoms. All structures are minimized and equilibrated with a *NPT* (isothermal-isobaric) ensemble set to a temperature of 300 K and a pressure of 1 atm. A time step of 1 femtosecond is used for each simulation, with a total simulation time ranging from 1.5 to 3 ns; the simulations are stopped when the structure

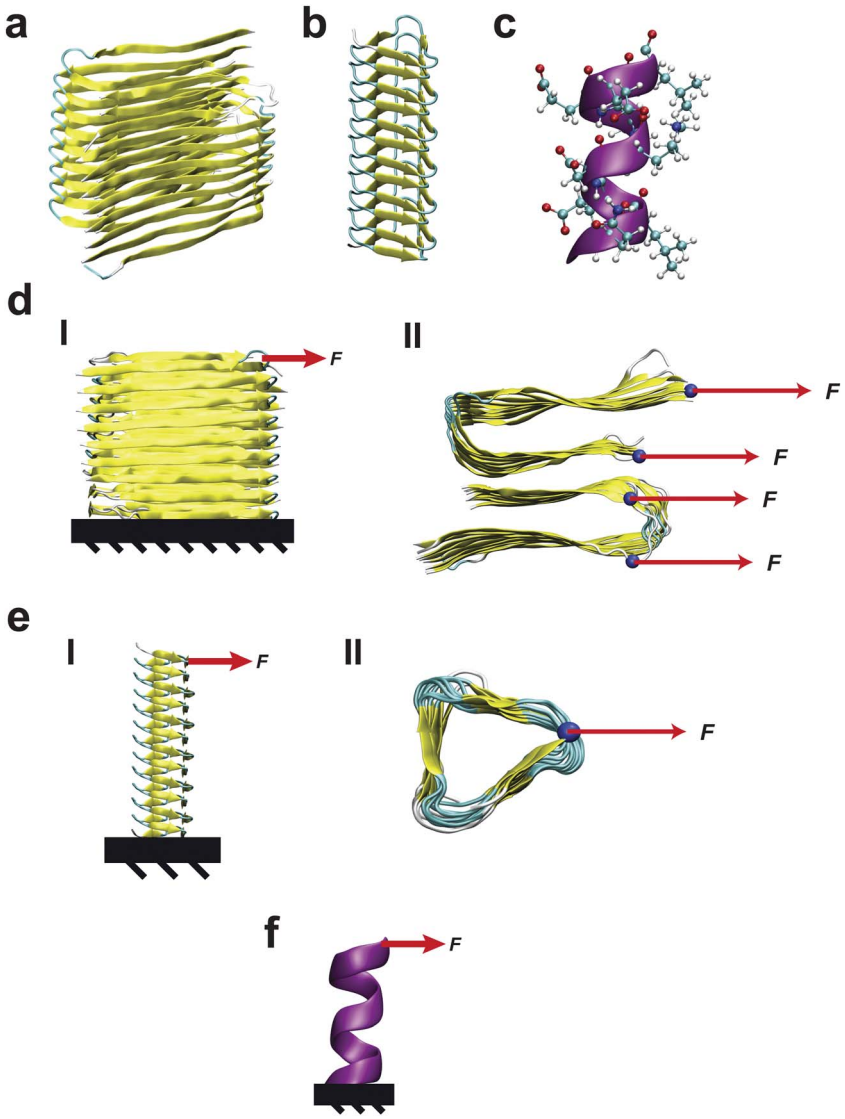

Fig. 1 Protein structures and loading conditions considered in this study. Panels (a)–(c) show representative structures for an Aβ(1–40) amyloid fibril, a β-helical nanotube, and an alpha helix, respectively. Panels (d)–(f) show how the loading conditions are applied. The atoms highlighted in blue in panel (d-II) and (e-II) are those to which the force is applied. For the alpha helix, the force is applied to the terminal C_α atom.

reaches a stable configuration. The stability of all structures is verified from root-mean-square deviation (RMSD) data from the molecular dynamics trajectory; all structures are considered equilibrated once the RMSD has plateaued for at least 0.5 ns. The simulations are carried out on both a 12 core Linux workstation and a 196 core Linux cluster at MIT's LAMM; up to 12 cores are used in a single simulation.

2.2 Loading conditions

All three structures are subjected to loading conditions similar to those of a cantilever beam under constant tip loading. For the Aβ (1–40) fibrils, the motion of the C_α atoms in the bottom layer is constrained and a constant force is applied to four C_α atoms in the top layer as illustrated in Fig. 1(d). For the β-helix and alpha helix structures, the C_α atoms in the bottom turn of the helix are held fixed and a constant force is applied to one C_α atom in the top turn as shown in Fig. 1(e) and 1(f). The choice of C_α atoms for the application of the loading boundary conditions is based on the goal of probing the mechanical response of the overall protein structure. Since the C_α atoms comprise the protein backbone, applying the forces to these atoms allows for some degree of consistency across the different structures considered, and it also prevents any effects that could arise from restricting the motion of side-chain groups.

For each structure, an appropriate force is chosen in order to generate adequate bending deformation while not resulting in failure. The forces applied range from 20 pN for the alpha helix up to 400 pN for the shortest (and stiffest) Aβ structure. These force levels are on the same order of magnitude as those applied in AFM protein unfolding experiments.[27] The tip displacement and bending profile measurements are performed once the structure has equilibrated under the applied load; equilibration is verified from root-mean-square deviation data. To reduce the effects of thermal fluctuations, atom positions are averaged over the final 100 simulation steps when calculating tip displacements and bending profiles.

2.3 Continuum theory and bending analysis

We undertake a similar analysis as reported in ref. 28, incorporating shear deformation effects in an extended beam model[29] to describe the behavior of the different protein structures considered. In this model, the displacement of the tip is given by:

$$\delta_{tip} = \frac{PL}{D_t} + \frac{PL^3}{3D_b} \tag{1}$$

where P is the applied load, $D_b = EI$ is the bending rigidity, and $D_t = GA$ is the shear rigidity. The effective bending stiffness is given by:

$$k_{eff}(L) = \frac{P}{\delta_{tip}} = \left(\frac{L}{D_t} + \frac{L^3}{3D_b}\right)^{-1}. \tag{2}$$

For comparison, we also perform an analysis based on classical beam theory without any shear effects (pure bending). For this model, the tip displacement is given by:

$$\delta^*_{tip} = \frac{PL^3}{3D_b} \tag{3}$$

and the bending stiffness is given by:

$$k^*_{eff}(L) = \frac{P}{\delta^*_{tip}} = \frac{3D_b}{L^3}. \tag{4}$$

The ratio of the two terms in eqn (1):

$$s = \frac{3D_b}{L^2 D_t} \tag{5}$$

gives a quantification of the importance of shear effects in the bending deformation; when s is less than one, pure bending cannot adequately describe the behavior, but when is greater than one, pure bending theory will suffice. The length for which s is equal to one gives an approximation for the critical length at which this transition occurs.

The effective stiffnesses from tip displacement for both the extended beam model (eqn (2)) and the pure bending model

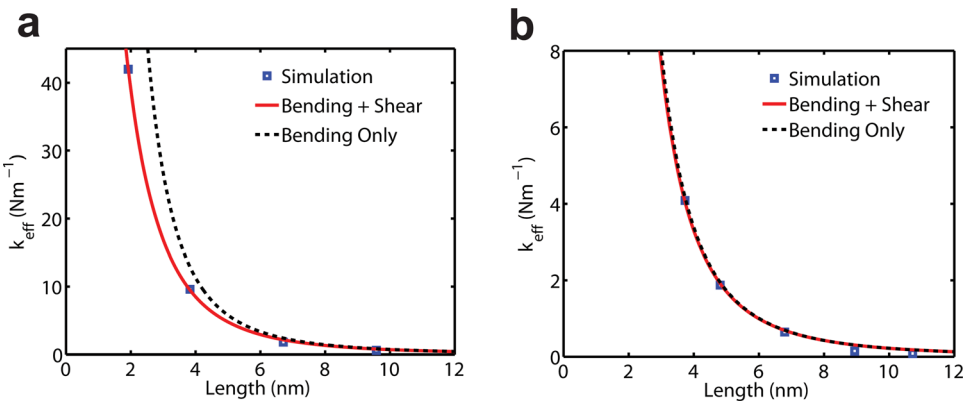

Fig. 2 Effective bending stiffness as a function of length for (a) amyloid fibrils and (b) β-helices. The curve labeled "Bending + Shear" is fit from eqn (2) (extended beam model) and the curve labeled "Bending Only" is fit from eqn (4) (pure bending model). The divergence of the two curves in (a) shows the predominance of shear deformation in the amyloid structure for shorter lengths. In panel (b) the curves for pure bending and bending with shear are indistinguishable for all lengths considered, illustrating that shear deformation does not play a role in the bending deformation of the β-helix structure. The difference in behavior between (a) and (b) is due to the structural differences between the amyloid fibrils and the β-helices. In the amyloid fibrils, individual layers are only held together by weak hydrogen bonds and are easily sheared. The β-helix structure has a continuous, covalently bonded backbone, which in addition hydrogen bonds between turns, provides an additional layer of interaction.

(eqn (4)) are plotted in Fig. 2 for each structure. Values of D_b and D_t are fitted to the data, allowing for the estimation of material properties (E,G and the persistence length $\xi = EI/k_BT$).[30] A simple geometric analysis of the atomic coordinates is used to calculate I and A for each structure; our calculated moment of inertia for the Aβ structure agrees well with experimental findings,[31] but we were unable to find experimental values for the other parameters for comparison and therefore we rely on the geometric analysis. Bending profiles are plotted in Fig. 4, with the solid curves calculated from:

$$\delta(y) = \frac{Py}{D_T} + \frac{P}{D_B}\left(\frac{Ly^2}{2} - \frac{y^3}{6}\right), \quad 0 \le y \le L \tag{6}$$

As done in [28] the values of D_b and D_t are further refined from the original fit for each case, but are kept within the 95% confidence range of the original fit from the tip displacement.

Fluctuations in the bending response of all three structures are analyzed by recording the value of the tip displacement over the final 100 simulation steps. Gaussian curves are fit to the data in order to provide a quantitative measure of the fluctuations in the three structures.

3. Results and discussion

Fig. 2 plots the effective bending stiffness as a function of length for both the Aβ (1–40) amyloid fibrils and the β-helix structure. The simulation results are plotted along with curves showing predictions from both the extended beam model and the pure bending model. It is evident from Fig. 2(a) that for the amyloid structure, shear effects must be included to accurately describe

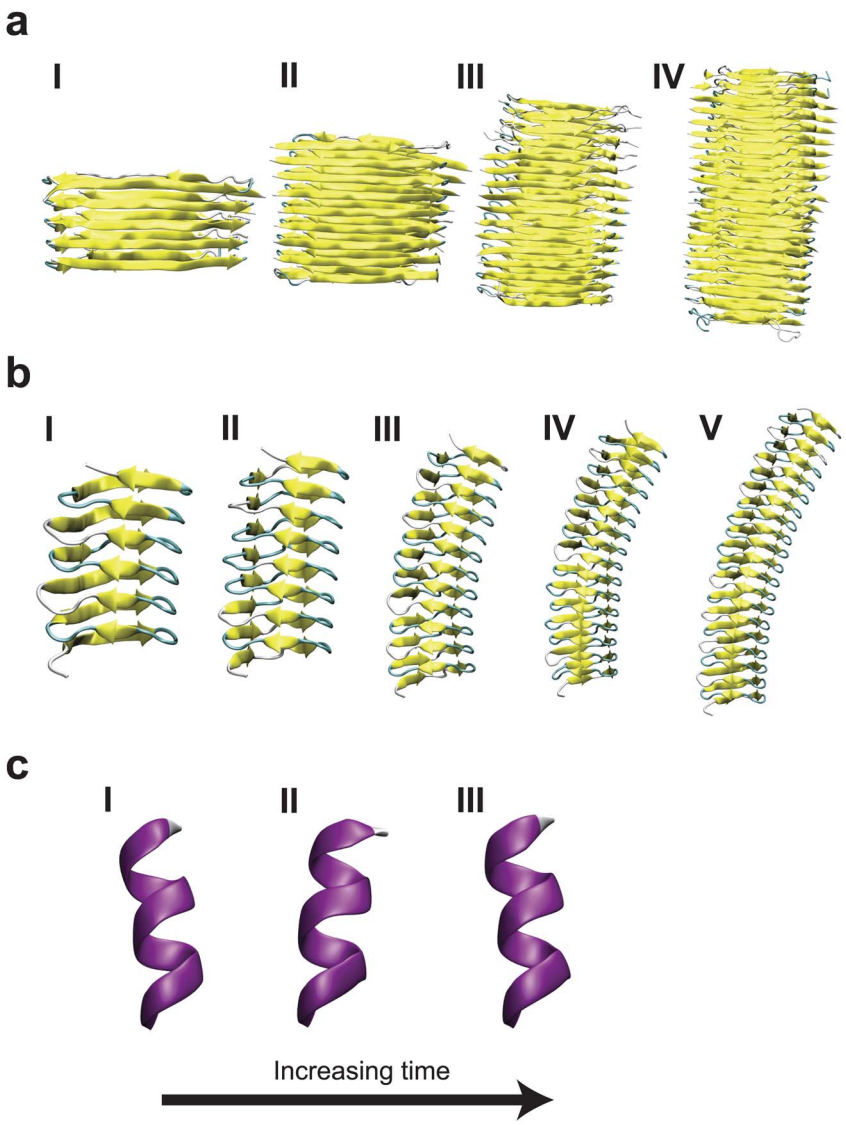

Fig. 3 (a) and (b) show simulation snapshots of the bending deformation profiles for the different sizes of amyloid fibrils and β-helices considered. The smaller amyloid structures in panel (a) feature a more linear strain distribution due to the larger shear contribution, while a nonlinear strain distribution consistent with bending deformation can be seen in even the smallest structure in (b). Panel (c) shows three snapshots of the alpha helix under constant lateral loading from the same simulation trajectory. The entropically driven behavior of the alpha helix can be seen in the back and forth motion of the structure under constant force.

the bending behavior, and they are most important for shorter fibrils. For the smallest fibril considered in this study, shear accounts for approximately 60% of the total deformation. From the values of D_b and D_t calculated from the fit, the critical length at which shear deformation is predominant in the amyloid structure is approximately 2.3 nm (about 6–7 layers). Shear deformation has been shown to be important for describing the mechanical behavior in many other hierarchically organized structures. Materials such as bone, microtubules and collagen all feature shear dependent deformation at different length scales; in particular, β-sheet nanocrystals in silk feature a structure similar to the amyloid, and exhibit similar shear dominated deformation for small lengths.[28,32–34]

In contrast, shear effects in the β-helix structure are rather unimportant. As seen in Fig. 2(b), the curves for both bending models are virtually indistinguishable; pure bending describes the behavior of the β-helix very well. Furthermore, shear effects would not become important until the length of the β-helix structure is reduced to a value less than the length of a single turn ($L \sim 0.6$ nm). The stark difference in bending behavior between the two β-sheet rich structures is explained by the differences in their structural organization. The amyloid structure comprises individual layers that are held together only by weak hydrogen bonds, and thus the layers are easily sheared. The β-helix structure, however, has a continuous, covalently bonded backbone, which provides an additional degree of resistance to shear deformation.

Fig. 3(a) and 3(b) show a series of simulation snapshots of the deformation profiles of the different sizes of amyloid fibrils and β-helices considered in this study. A simple visual comparison of the bending behavior of the two structures illustrates the difference between shear-dominated deformation in the Aβ fibrils and pure bending in the β-helices, especially for shorter lengths. Fig. 4 (a) and 4(b) plot the displacement profiles for each case. The solid curves show the continuum theory predictions from eqn (6).

In addition to the analysis of the importance of shear, material properties are estimated from D_b and D_t For the amyloid fibril, we find the Young's Modulus $E = 9.9$ GPa the bending rigidity $EI = 2.41 \times 10^{-25}$ Nm^2. These findings are in good agreement with previous simulation results[9,10,13,15,31] as well as experimental results[31,35,36] which find E in the range of 10 to 30 GPa and EI in the range of 0.1×10^{-25} to 2.5×10^{-25} Nm^2. We also find the shear modulus $G = 10.2$ GPa for the amyloid fibril. This value is close to simulation results,[15] which report a shear modulus of 5.6 GPa for Aβ(1–40) amyloid fibrils; the higher modulus reported here is possibly due to differences in loading conditions and simulation techniques, however the difference (~5 GPa) is smaller than the spread in the experimentally measured values of

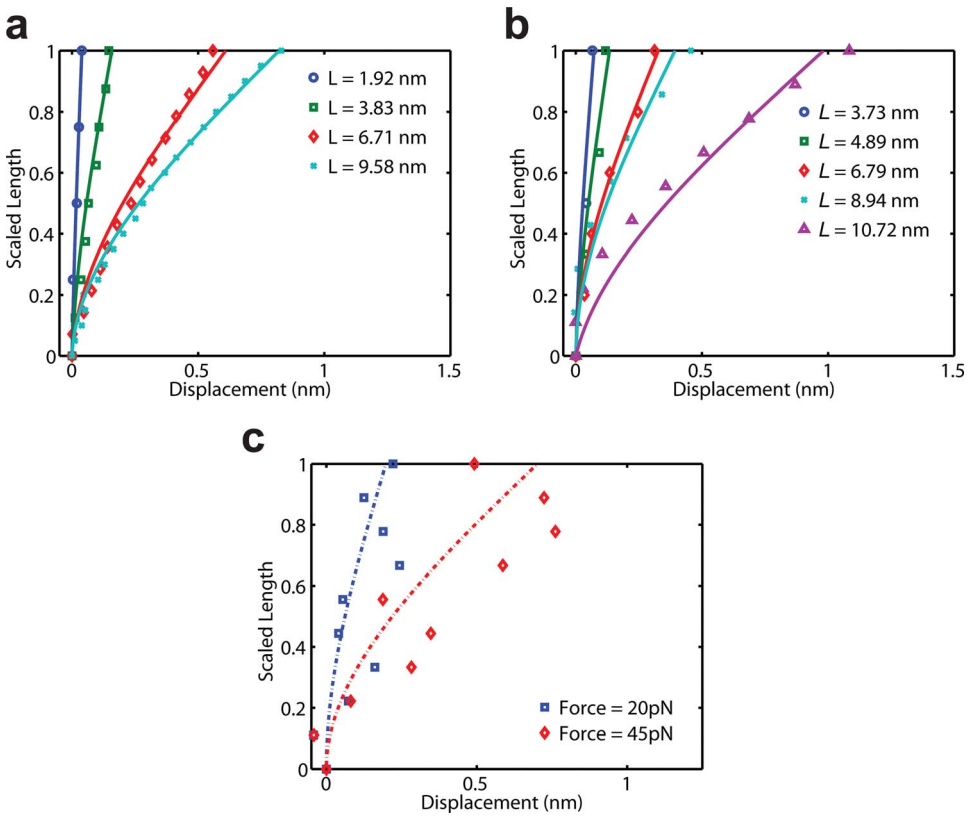

Fig. 4 Bending profiles for the three structures considered in this study. Panel (a): Amyloid fibril. Panel (b): β-helix, and panel (c): Alpha helix. The solid curves in (a) and (b) show fits based on continuum theory (eqn (6)), and in general, the results agree quite well with the theory. The deformation profiles for the alpha helix structure for two different loads are shown in panel (c). The highly non-uniform nature of the deformation profiles illustrates the predominance of statistical fluctuations in the bending behavior. The dashed lines show fits to the profiles from eqn (6) without the inclusion of the shear term (pure bending). The predicted bending rigidity from these fits is overestimated by up to two orders of magnitude (compared with experimental data), further illustrating that the classical continuum mechanical theory cannot be applied to describe the deformation behavior of the alpha helix structure.

Table 1 Summary of geometric parameters used as well as mechanical properties extracted from this study

Parameter/Property			Structure		
			Aβ(1–40) Amyloid Fibril	β-helix	Alpha Helix
Cross-sectional Area	A (m^2)		1.34×10^{-17}	—	—
Second Moment of Area	I (m^4)		2.52×10^{-35}	2.13×10^{-36}	—
Young's Modulus	E (GPa)	This Study	9.9	29.1	—
		Previous Work	10–30[9,10,13,15,31,35,36]	26.4[34]	—
Shear Modulus	G (GPa)	This Study	10.2	—	—
		Previous Work	5.6[15]	—	—
Bending Rigidity	EI (Nm^2)	This Study	2.41×10^{-25}	6.2×10^{-26}	$2–4 \times 10^{-28}$[a,c]
		Previous Work	0.1×10^{-25}–2.5×10^{-25}[9,10,13,15,31,35,36]	—	$\sim 4 \times 10^{-30}$[b]
Persistence Length	ξ	This Study	~60μm[a]	~15μm[a]	~60–100nm [a,c]
		Previous Work	0.5–100 μm[5,13]	1.4 μm[17]	~1nm[38]

[a] These values are calculated from the bending rigidities found in this study. [b] This value is calculated from the persistence length reported in ref. 38. [c] These values are expected to disagree with literature findings. Since they are based on fits to continuum theory, the fact that they disagree to such a large extent further supports the idea that the continuum theory cannot be used to describe the mechanical response of the alpha helix with a length greater than its persistence length.

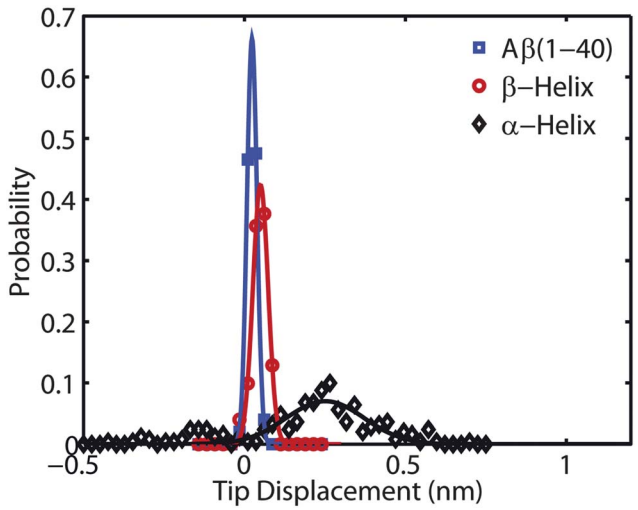

Fig. 5 Fluctuation analysis for the three structures considered. The tip displacement distributions are plotted as well as Gaussian fits. The amyloid and β-helix structures exhibit some small fluctuations (~0.1 nm) in the tip displacement over the simulation trajectory, however the tip displacement for the alpha helix structure is much larger, spanning over 1nm. This analysis demonstrates that for the Amyloid and β-helix structures with lengths well below their persistence lengths, fluctuations play a negligible role in describing mechanical response. In contrast, the deformation behavior of the alpha helix is dominated by fluctuations; continuum theory, which does not account for these fluctuations, can not provide an accurate description of the mechanical response of the alpha helix.

the Young's modulus (~20 GPa as indicated above). For the β-helical nanotube, we find the Young's modulus $E = 29.1$ GP and the bending stiffness $EI = 6.2 \times 10^{-26}$ Nm^2. Our findings agree well with previous results which find $E = 26.4$ GPa.[37] Due to the very small contribution of shear in the bending deformation of the β-helix structure, its shear modulus cannot be reliably extracted from our findings. The material properties extracted from this study are summarized in Table 1.

A final analysis of deformation behavior of protein filaments is made on the basis of persistence length. Broadly, the persistence length provides a limiting length scale above which statistical/entropic fluctuations dominate and continuum mechanics does not well describe the deformation behavior. To examine this directly, we compare the behavior of the two β-sheet rich proteins, both with lengths on the order of 1–10 nm and $\xi > 1$ μm, to that of an alpha helix with a length of 2.3 nm and $\xi \sim 1$nm.[38] As established through the analyses above, both β-sheet rich structures are well described by continuum theory. The alpha helix, however, is not. Fig. 3(c) shows three snapshots from the lateral loading simulation of the alpha helix. Although a constant force is applied, the alpha helix moves back and forth erratically over the simulation trajectory. Fig. 4(c) plots the average deformation profile of the alpha helix over the final 250 ps of the simulation for two different applied loads. Both profiles show the highly non-uniform bending behavior that originates from the large influence of entropic effects. The dashed curves in Fig. 4 (c) show fits to the bending profiles based on eqn (3). The bending rigidities obtained from these fits are $EI = 4 \times 10^{-28}$ Nm^2 and $EI = 2 \times 10^{-28}$ Nm^2 for the 20pN and 45pN force levels, respectively. Based on a persistence length of 1 nm, however, the bending rigidity of the alpha helix should be $\sim 4 \times 10^{-30}$ Nm^2, a factor of up to 100 smaller than the values obtained from the continuum theory fits. This large discrepancy again demonstrates that the continuum theory cannot be used to describe the mechanical behavior of the alpha helix.

Fig. 5 shows the distribution of tip displacements over the final 100 simulation steps for the three structures considered in this study (the distributions shown for the amyloid fibril and β-helix are for the shortest length of each structure); a Gaussian function is fit to each distribution. We find that the fluctuations in the tip distribution for the amyloid fibril and the β-helix are quite small; the standard deviations of both distributions are approximately 0.05 nm (smaller than one Angstrom, the characteristic length of typical chemical bonds). In contrast, the distribution for the alpha helix spans a much larger range of tip displacements, and the standard deviation of approximately 0.5 nm. This distribution is consistent with the emergence of entropic elasticity, where the deformation behavior is dominated by fluctuations. This fluctuation analysis further shows that continuum mechanical theory breaks down for length scales that exceed the persistence length of filamentous protein structures, and that in this regime,

the mechanical response can only be described by theories that incorporated statistical effects.[39]

4. Conclusions

Our results provide insight into the ways in which protein secondary structure type, size, and organization, affect mechanical behavior and properties. They also illustrate key differences in deformation behavior that arise from different structural motifs. We find that both amyloid fibrils and β-helical nanotubes, with predominantly β-sheet secondary structures and lengths well below their persistence lengths, are very well described by continuum mechanical theory. For the amyloid structure, the inclusion of shear deformation in the overall description of the bending behavior is essential owing to the fact that the hydrogen bonded β-sheet layers are easily sheared. The behavior of the β-helix structure, however, can be described with just the contribution from pure bending. The continuous, covalently bonded backbone of the β-helix prevents significant shear deformation under lateral tip loading. Further, mechanical properties calculated from our study are in good agreement with previous computational and experimental results (Table 1).

Our comparison of behavior on the basis of persistence length is very much in line with theoretical predictions. The two structures studied with lengths below their persistence length feature deformation behavior consistent with continuum theory, while the alpha helix structure with a length greater than its persistence length is characterized by more erratic behavior dominated by statistical (entropic) fluctuations. We find the persistence length to be an excellent metric for separating length scales at which continuum theory is applicable, and those for which a statistical treatment must be used to describe mechanical response.[39]

The analysis presented here could be directly applied to a host of other protein, polymer, or inorganic structures including DNA, metallic nanowires or carbon nanostructures, and could both further our understanding of numerous biological processes or aid in the design of *de novo* functional materials.

Acknowledgements

Support from ONR (N000140810844) and NSF (CMMI-0642545) is acknowledged.

References

1 G. E. Schulz and R. H. Schirmer, *Principles of protein structure*, Springer-Verlag, New York, 1979.
2 K. Wuthrich, *Science*, 1989, **243**, 45.
3 L. Pauling, R. B. Corey and H. R. Branson, *Proc. Natl. Acad. Sci. U. S. A.*, 1951, **37**, 205.
4 F. Chiti and C. M. Dobson, *Annu. Rev. Biochem.*, 2006, **75**, 333.
5 T. P. J. Knowles and M. J. Buehler, *Nat. Nanotechnol.*, 2011, **6**, 469.
6 C. M. Dobson and C. E. MacPhee, *J. Am. Chem. Soc.*, 2000, **122**, 12707.
7 D. N. Woolfson and C. E. MacPhee, *Curr. Opin. Solid State Mater. Sci.*, 2004, **8**, 141.
8 R. Paparcone and M. J. Buehler, *Appl. Phys. Lett.*, 2009, **94**, 243904.
9 R. Paparcone and M. J. Buehler, *JOM*, 2010, **62**, 64.
10 R. Paparcone and M. J. Buehler, *Biomaterials*, 2011, **32**, 3367.
11 R. Paparcone, S. Cranford and M. J. Buehler, *Acta Mech. Sin.*, 2010, **26**, 977.
12 R. Paparcone, S. W. Cranford and M. J. Buehler, *Nanoscale*, 2011, **3**, 1748.
13 R. Paparcone, S. Keten and M. J. Buehler, *J. Biomech.*, 2010, **43**, 1196.
14 R. Paparcone, M. A. Pires and M. J. Buehler, *Biochemistry*, 2010, **49**, 8967.
15 Z. P. Xu, R. Paparcone and M. J. Buehler, *Biophys. J.*, 2010, **98**, 2053.
16 D. L. Cox, H. Lashuel, K. Y. C. Lee and R. R. P. Singh, *MRS Bull.*, 2005, **30**, 452.
17 S. Keten and M. J. Buehler, *Comput. Methods Appl. Mech. Eng.*, 2008, **197**, 3203.
18 T. Ackbarow and M. J. Buehler, *J. Mater. Sci.*, 2007, **42**, 8771.
19 R. Paparcone, J. Sanchez and M. J. Buehler, *J. Comput. Theor. Nanosci.*, 2010, **7**, 1279.
20 F. C. Bernstein, T. F. Koetzle, G. J. B. Williams, E. F. Meyer, M. D. Brice, J. R. Rodgers, O. Kennard, T. Shimanouchi and M. Tasumi, *J. Mol. Biol.*, 1977, **112**, 535.
21 K. Brown, F. Pompeo, S. Dixon, D. Mengin-Lecreulx, C. Cambillau and Y. Bourne, *EMBO J.*, 1999, **18**, 4096.
22 S. V. Strelkov, H. Herrmann, N. Geisler, T. Wedig, R. Zimbelmann, U. Aebi and P. Burkhard, *EMBO J.*, 2002, **21**, 1255.
23 Z. Qin, A. Fabre, and M. J. Buehler, in submission.
24 W. Humphrey, A. Dalke and K. Schulten, *J. Mol. Graphics*, 1996, **14**, 33.
25 M. T. Nelson, W. Humphrey, A. Gursoy, A. Dalke, L. V. Kale, R. D. Skeel and K. Schulten, *Int. J. High Perform. Comput. Appl.*, 1996, **10**, 251.
26 A. D. MacKerell, D. Bashford, M. Bellott, R. L. Dunbrack, J. D. Evanseck, M. J. Field, S. Fischer, J. Gao, H. Guo, S. Ha, D. Joseph-McCarthy, L. Kuchnir, K. Kuczera, F. T. K. Lau, C. Mattos, S. Michnick, T. Ngo, D. T. Nguyen, B. Prodhom, W. E. Reiher, B. Roux, M. Schlenkrich, J. C. Smith, R. Stote, J. Straub, M. Watanabe, J. Wiorkiewicz-Kuczera, D. Yin and M. Karplus, *J. Phys. Chem. B*, 1998, **102**, 3586.
27 M. Kawakami, K. Byrne, D. J. Brockwell, S. E. Radford and D. A. Smith, *Biophys. J.*, 2006, **91**, L16.
28 S. Keten, Z. P. Xu, B. Ihle and M. J. Buehler, *Nat. Mater.*, 2010, **9**, 359.
29 J. J. Connor, *Introduction to structural motion control*, Prentice Hall Pearson Education, Inc., Upper Saddle River, N.J., 2003.
30 P. J. Flory, *Statistical mechanics of chain molecules*, Interscience Publishers, New York, 1969.
31 T. P. Knowles, A. W. Fitzpatrick, S. Meehan, H. R. Mott, M. Vendruscolo, C. M. Dobson and M. E. Welland, *Science*, 2007, **318**, 1900.
32 M. J. Buehler, *Proc. Natl. Acad. Sci. U. S. A.*, 2006, **103**, 12285.
33 M. A. Deriu, M. Soncini, M. Orsi, M. Patel, J. W. Essex, F. M. Montevecchi and A. Redaelli, *Biophys. J.*, 2010, **99**, 2190.
34 P. Fratzl and R. Weinkamer, *Prog. Mater. Sci.*, 2007, **52**, 1263.
35 N. Kol, L. Adler-Abramovich, D. Barlam, R. Z. Shneck, E. Gazit and I. Rousso, *Nano Lett.*, 2005, **5**, 1343.
36 J. F. Smith, T. P. J. Knowles, C. E. MacPhee, M. E. Welland and C. M. Dobson, *Proc. Natl. Acad. Sci. U. S. A.*, 2006, **103**, 15806.
37 Z. P. Xu and M. J. Buehler, *Phys. Rev. E*, 2010, **81**.
38 P. Papadopoulos, I. Schnell, I. Lieberwirth, T. Q. Nguyen, H. A. Klok and G. Floudas, *Biomacromolecules*, 2006, **7**, 618.
39 T. Su and P. K. Puohit, Fluctuating elastic filaments under distributed loads, *Mol. Cell. Biomech.*, 2011, **8**, 215.